Droop Integrated Distribution Grid Power Flow

Aashutosh Neupane and Sumit Paudyal
Florida International University, USA
Emails: {aneup003, spaudyal}@fiu.edu

***Abstract*—Over the past years, considerable effort has been directed toward the formulation and solution of distribution system power flow. These efforts have led to the development of promising power flow models, algorithms, and open-source tools such as OpenDSS and GridLAB-D, capable of modeling and solving unbalanced power flow in large-scale distribution systems. In modern distribution grids, the deployment of power-electronics-based devices, such as smart inverters (SIs), is increasing. These devices can control active and reactive power injection at the point of common coupling (PCC) and typically operate based on local piecewise droop functions, e.g., $P(V)$, $Q(V)$. Integration of SI droop settings into the power flow formulation is essential, as ignoring them can result in power flow solutions that can violate the SIs' droop characteristics. Therefore, this work is focused to develop a droop-integrated power flow model and solution method for unbalanced distribution systems. The effectiveness of the proposed model and solution approach is demonstrated through case studies conducted on the IEEE 123-node test feeder upto 67 SIs.**

***Index Terms*—Photovoltaics, Distribution Network, Smart Inverters, Droop Setting, Active Distribution Network, Powerflow**

I. Introduction

Advances in smart inverter (SI) technology have significantly enhanced the functionality of distributed photovoltaic (PV) resources in modern distribution grids, enabling not only resiliency-oriented modes such as grid-forming and grid-following but also participation in ancillary services through advanced control features [1]. As PV continues to be the fastest-growing distributed energy resource (DER) worldwide [2], its increasing penetration can lead to reverse power flow, voltage rise, and rapid voltage fluctuations [3]. These challenges make voltage regulation a major task for distribution management systems, which must increasingly rely on coordinated SI capabilities to maintain voltages within operational limits and ensure reliable network operation.

The inherently high R/X ratio of distribution feeders increases the sensitivity of bus voltages to reverse power flow during periods of significant PV generation. Although conventional voltage regulation equipment is being upgraded for future grid needs, such devices may still fall short in responding quickly or adequately to the rapid variability of PV output. In contrast, power-electronic based SIs can provide fast Volt/VAr regulation. Consequently, local droop-based controls as specified in IEEE-1547 [4], including functions like Volt-VAr $(\mathbf{Q}(\mathbf{V}))$, Volt-Watt $(\mathbf{P}(\mathbf{V}))$, Watt-VAr $(\mathbf{Q}(\mathbf{P}))$, and Watt–power factor $(\cos\phi(\mathbf{P}))$ [5], offer practical and efficient means to mitigate PV-related voltage issues and supply rapid reactive power support based on local control at SI end. This standardization enables utilities to move beyond simply accommodating DERs toward actively leveraging them as grid assets. They can also provide ancillary services through autonomous droop-based functions [6]. Combining reactive power support via Volt-VAr control $(\mathbf{Q}(V))$ with active power curtailment via Volt-Watt control $(\mathbf{P}(V))$ is particularly effective for alleviating overvoltage and expanding PV hosting capacity as PV penetration continues to increase [7].

As these SI functions are becoming fundamental to distributed PV operation, utilities must enhance their distribution management system (DMS) applications to coordinate inverter behavior reliably and at scale. Incorporating such capabilities requires representation and systematic modeling of droop-based function within DMS decision-making framework such as distribution power flow and distribution optimal power flow (DOPF). Prior works such as [8]–[10] have used models to schedule active and reactive power from SIs to reduce losses and mitigate voltage violations. However, IEEE-1547 mandates that SIs follow their local droop settings [4], and many existing power flow or DOPF models do not include these mandatory local droop settings of SIs. Consequently, the derived SI setpoints based on existing power flow or DOPF models may conflict with local droop-based SI control, making them impractical at the device level. Ensuring system-level feasibility without violating IEEE-1547 therefore requires embedding SI droop characteristics directly into power flow formulations. Attempts have been carried out in integrating SIs's droop on DOPF formulation in the literature [11], [12], however a limited work exists that integrates droop function while solving power flow [13]. As the existing literature has focused on modeling and solving optimization models with droop functionalities or the AC power flow modeling and solution that only considers DER set points, there hasn't been much exploration in using the droop setting incorporated power flow formulation. This work develops a power flow formulation and solution process in unbalanced distribution systems with droop functions of SIs.

The remainder of the paper is organized as following. Section II presents the mathematical formulations involved, Section III presents the numerical analysis, and Section IV

This work is supported by the U.S. Department of Energy's Office of Energy Efficiency and Renewable Energy (EERE) under the Solar Energy Technologies Office Award Number DE-EE0011369. Corresponding Author: A. Neupane (email: aneup003@fiu.edu).

979-8-3315-8138-1

concludes the paper with potential directions for future research.

II. Mathematical Modeling

A. Radial Distribution Network

The radial power distribution feeder can be represented as the unidirectional and connected graph $\mathcal{G}$ =$(\mathcal{N}, \mathcal{E})$, with n nodes, where $\mathcal{N}$: $\{0, 1, 2, ..., n\}$ is the set of all the nodes of the network and $\mathcal{E} \subseteq \mathcal{N} \times \mathcal{N}$, where $\mathcal{E}$ represents the set of the distribution lines that connects the ordered pair of buses (i, j) from node $i \rightarrow j$ where the term (i, j) and $i \sim j$, $i \neq j$ is used interchangeably to denote the link in $\mathcal{E}$. The admittance matrix Y is defined as $(n + 1) \times (n + 1)$ and can be represented as:

$$Y_{ij} = \begin{cases} \sum\limits_{k \sim i} y_{ik}, & \text{if } i = j, \\ -y_{ij}, & \text{if } i \neq j \text{ and } i \sim j, \\ 0, & \text{otherwise.} \end{cases} \tag{1}$$

Y matrix is symmetric but not necessarily a Hermitian matrix. The complex voltage on bus i is denoted by V_i for $i \in \mathcal{N}$. The net complex power injection and current is defined as $\tilde{S}_i$ and $\tilde{I}_i$, respectively, at bus i into the distribution network. The network model in bus injection form can be written as,

$$\tilde{I} = YV \tag{2}$$

$$\tilde{S}_i = V_i \tilde{I}_i^*, \quad i \in \mathcal{N} \tag{3}$$

$$s_i = -\tilde{S}_i, \quad i \in \mathcal{N} \tag{4}$$

When the V_o voltages and s_i are known, where $i = 1, 2, ...n$, the network variables such as ($\tilde{S}_i$,$\tilde{I}_i$,V,s_o) can be calculated that satisfies (2)-(4).

B. Smart Inverter Control

SIs interfaced with the PV systems is capable of delivering both active and reactive power per phase at the point of common coupling (PCC), in the distribution grid. These SIs can provide dynamic reactive support to the grid, but the total reactive support that SIs can supply is constrained by the apparent power rating of the SI connected at each node. The available reactive power $q^p_{pv,i}$ from the SI can be represented mathematically as in (5).

$$-\sqrt{\left(S^{\text{rated},p}_{\text{pv},i}\right)^2 - \left(P^p_{\text{pv},i}\right)^2} \leq q^p_{\text{pv},i} \leq \sqrt{\left(S^{\text{rated},p}_{\text{pv},i}\right)^2 - \left(P^p_{\text{pv},i}\right)^2} \tag{5}$$

Here, $S^{\text{rated},p}_{\text{pv},i}$ denotes the apparent power capacity of the SI connected to the i^{th} node of the distribution network and $P^p_{\text{pv},i}$ denotes the generated active power by the SI.

C. Volt-VAr Droop

In reactive power priority mode, $\boldsymbol{Q(V)}$, the SI regulates the voltage either by injecting or absorbing reactive power bidirectionally. The reactive power output depends on the local voltage at the PCC. As illustrated in Fig. 1, $\boldsymbol{Q(V)}$ droop follows a piecewise-defined function in terms of PCC voltage as,

$$Q_{pv}(V^i_{pv}) = \begin{cases} Q_1, & V^i_{pv} \leq V_1 \\ \gamma_2(V^i_{pv} - V^i_2), & V^i_1 < V^i_{pv} \leq V^i_2 \\ 0, & V^i_2 < V^i_{pv} \leq V^i_3 \\ \gamma_4(V^i_{pv} - V^i_3), & V^i_3 < V^i_{pv} \leq V^i_4 \\ Q_4, & V^i_{pv} > V_4 \end{cases} \tag{6}$$

$$\gamma_{\min} \leq \gamma_2, \gamma_4 \leq \gamma_{\max};$$

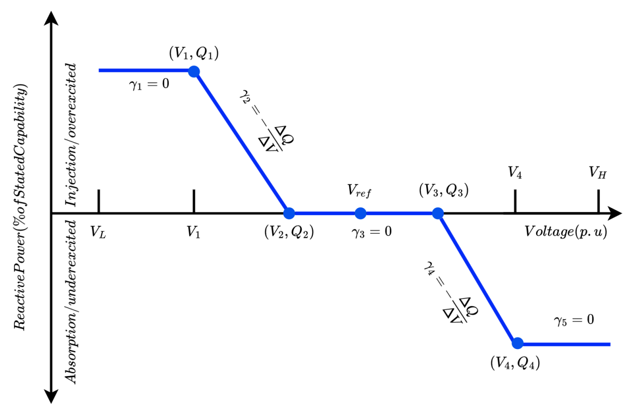

Fig. 1: Smart Inverter Q(V) droop curve [14].

SI injects rated reactive power, Q_1 (denoted as $Q^{injection}_{max}$), when the PCC voltage of the PV (V^i_{pv}) at the connected node i is within $V_L \leq V^i_{pv} \leq V_1$. The output of the reactive power from the SI is curtailed along the two slopes $\boldsymbol{\gamma_2}$ and $\boldsymbol{\gamma_4}$ over the intervals $V_1 \leq V^i_{pv} \leq V_2$ and $V_3 \leq V^i_{pv} \leq V_4$, corresponding to reactive power injection and absorption, respectively. The dead-band is defined in the interval $V_2 \leq V^i_{pv} \leq V_3$, during which there is no reactive power from SIs. SI absorbs its maximum reactive power, Q_4 (denoted as $Q^{absorption}_{max}$), when the voltage is in the range $V_4 \leq V^i_{pv} \leq V_H$. The voltage setpoint for the $\boldsymbol{Q(V)}$ droop point in this work follows the IEEE 1547 Category B SI specifications, with the maximum reactive power injection and absorption set to 44% of the SI rating.

D. Volt-Watt Droop

SI is capable of operating in a combined mode, utilizing both the Volt-Watt (see Fig. 2) and Volt-VAr functions, to provide active power support at the PCC alongside with the reactive power while operating in the reactive power priority mode. The available active power that the SI can supply depends upon the SIs apparent rating as in (7)-(8). In coordinated control mode of the two settings, the active power injection is determined by the remaining capacity of

979-8-3315-8138-1

the SI after satisfying the reactive power output based on the voltage at PCC, which can be expressed as,

$$P_{pv}(V_{pv}^{i}) \leq P_{pv}^{\max} \tag{7}$$

$$P_{pv}^{\max} = \sqrt{S_{pv}^{2} - Q_{pv}(V_{pv}^{i})^{2}} \tag{8}$$

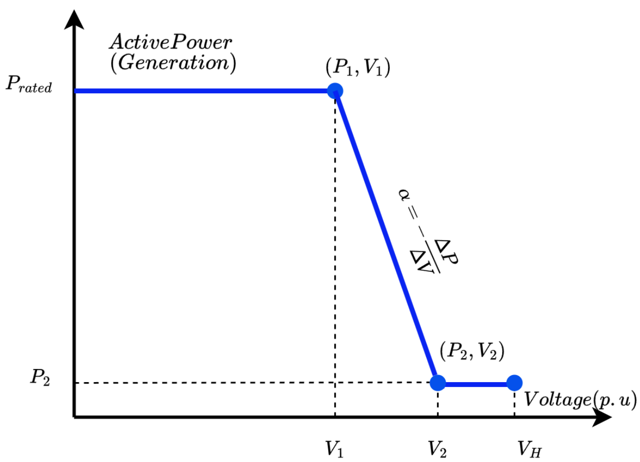

Fig. 2: Smart Inverter P(V) droop curve [14].

E. Droop Integrated Power Flow

A Reactive Power priority droop control model is embedded directly into the iterative Z-bus power flow method. The Algorithm 1 is developed as following,

Input: $Y_{\text{bus}}, Y_{\text{sub}}, V_{\text{sub}}^{\phi}, S_{\text{load,i}}^{\phi}, S_{\text{pv,i}}^{\phi}, \epsilon, N_{\max}$
Output: Converged $V_i^{\phi}, \delta^{\phi}$
Initialize $\mathbf{V}_i^{\phi} = V_{\text{init}}\angle\delta_{\text{init}},\ \forall i \in \mathcal{N}$, it=0, ϵ=10e^{-5}
while *error* $> \epsilon$ ***and*** *it* $< N_{\max}$ **do**
  $V_{\text{old}}^{\phi} \leftarrow V_1^{\phi},\ V_2^{\phi} \leftarrow |V_1^{\phi}|$;
  for $i \in \mathcal{N}_{\mathcal{DER}}$ **do**
    Compute $Q_{\text{pv},i}^{\phi}$ using (6)
    $P_{\text{pv},i}^{\phi} = \sqrt{(S_{\text{pv},i}^{\text{rated},\phi})^2 - (Q_{\text{pv},i}^{\phi})^2}$
    $I_{\text{DER},i}^{\phi} = \text{conj}\Big((P_{\text{pv},i} + j\,Q_{\text{pv},i})/V_i^{\phi}\Big)$
  end
  for $i \in \mathcal{N}$ **do**
    $IL_i^{\phi} = 0$ **if** $S_{\text{load,i}}^{\phi} = 0$
    else IL_i^{ϕ}=-conj$\Big((S_{\text{load},i}^{\phi}/V_i^{\phi}\Big)$
  end
  $I_{\text{net}}^{\phi} = IL_{4:\mathcal{N}}^{\phi} + I_{\text{DER},4:\mathcal{N}}^{\phi}$
  $V_{\mathcal{N}}^{\phi} = Y_{\text{bus}}^{-1}(I_{\text{net}}^{\phi} - Y_{\text{sub}}V_{\text{sub}}^{\phi})$
  $V^{\phi} = [V_{\text{sub}}^{\phi}, V_{\mathcal{N}}^{\phi}]$
  error $= \max\Big(|V_i^{\phi} - V_{\text{old,i}}^{\phi}|/|V_{\text{old,i}}^{\phi}|\Big)$
end

Algorithm 1: Droop Integrated Power Flow Solution Method.

III. Numerical Results

A. Base Case Power Flow

The Z bus-based power flow model is developed and first validated on the IEEE-123 Node test feeder (without SIs droop function) by comparing the results against the OpenDSS. The loads were converted to wye-connected constant power loads, and the network was solved with regulator tap set to zero. The voltage-magnitude and angle comparison between two models are shown Fig. 3 and Fig. 4, respectively.

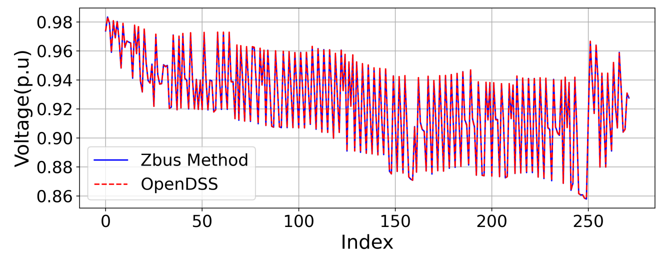

Fig. 3: Voltage Profile of the IEEE 123-node feeder.

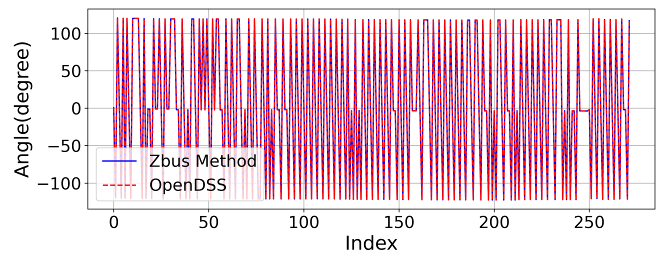

Fig. 4: Angles of the IEEE 123 node-feeder.

B. Iterative Solution Process with SI Droop Functions

The $\mathbf{Q}(\mathbf{V})$ priority droop integrated power flow solution is demonstrated using modified IEEE 123-node test feeder (see Fig. 5) with two SIs rated 300 kW and 150 kW, at Bus 42 (phase 'a') and at Bus 77 (phase 'b'), with droops based on the IEEE-1547. The results show $Q(V)$ and $P(V)$ droop curve to visualize the reactive and active power supplied by the SIs over each iteration of the solution process. The resulting $Q(V)$ plots are shown in Fig. 6, with detailed visualizations shown in Fig. 6a and Fig. 6c. During the beginning of the iterations, the SI operates within the dead band, supplying or absorbing no reactive power. As the iteration progresses, the operating point shifts along the piecewise-linear droop curve in response to the PCC voltage at each iterations step until the solution converges. The x-axis represents the per-unit (p.u) voltage at the PCC, while the y-axis indicates the percentage of the reactive power injection or absorption relative to the SIs rated capacity, with 44% being the maximum permissible injection/absorption set in this study. In the reactive priority mode, active power is supplied from the remaining SI capacity after satisfying the reactive power requirement, in accordance with (8). The Volt-Watt droop settings, that represent the active power output of the SI, are shown in Fig. 6b and Fig. 6d in accordance with the IEEE-1547. It can be inferred from this plots, that the SI supplies its maximum reactive power during the beginning of the iteration process when the Volt-VAr curve operates within the deadband region. The x-axis represents the voltage (p.u), while the y-axis indicates the % of the active power delivered by the SI relative to it's rated capacity. In this

979-8-3315-8138-1

case study, the convergence was achieved in 6 iterations. The program is capable of tracking the solutions at each iteration on Volt-VAr and Volt-Watt droops; however, if the solution doesn't change significantly between the iterations, data points may appear closer or even overlap.

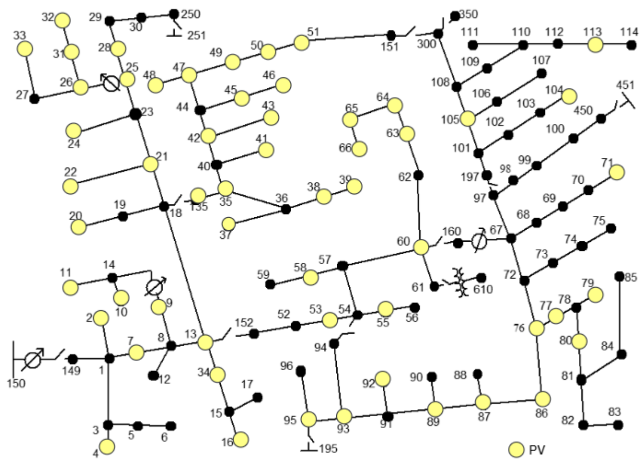

Fig. 5: Location of the PV in the IEEE 123 node test feeder.

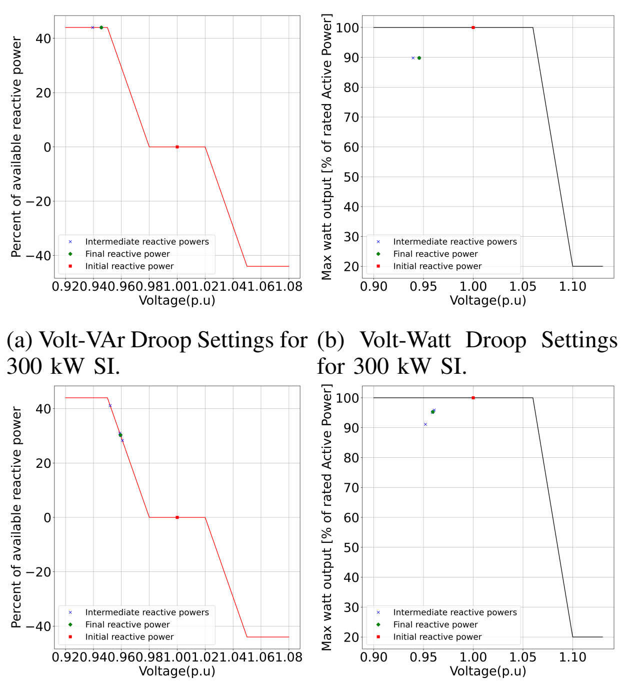

(a) Volt-VAr Droop Settings for 300 kW SI.

(b) Volt-Watt Droop Settings for 300 kW SI.

(c) Volt-VAr Droop Settings for 150 kW SI.

(d) Volt-Watt Droop Settings for 150 kW SI.

Fig. 6: Iterative Droop Convergence of SI at Bus 42 and 77.

C. High Penetration of Distributed Small Scale PVs

The droop integrated power flow algorithm is used to evaluate the effect of droop settings on the overall voltage profile of the IEEE-123 node feeder. Specifically, two droop control strategies for SIs are examined. First, a uniform droop setting is used, where all SIs in the distribution network operate with identical droop parameters. On the second strategy, the droop settings are non-uniform, where the droop setpoint values vary for each SI connected in the distribution network. The location of the 67 PVs connected to the feeder is illustrated in Fig. 5. The total PV capacity is 2.754 MW, distributed as 910 kW, 1030 kW and 814 kW installed in phase a, b and c, respectively, with individual units ranging from 25-100 kW. This case study evaluates two distinct SI Volt-VAr configurations, as summarized in Table I. The uniform droop settings follow the exact parameters in Table I, while the non-uniform settings are selected with arbitrary small changes on the parameters for each SIs. The resulting voltage profiles for both uniform and non-uniform droop settings are shown in Fig. 7 for Configuration 1 (Config 1) and Fig. 8 for Configuration 2 (Config 2).

TABLE I: Droop Setpoint for Smart Inverters

$S.N$	V_L	V_1	V_2	V_3	V_4	V_H
Configuration 1	0.90	0.92	0.95	0.98	1.02	1.05
Configuration 2	0.90	0.95	0.97	1.00	1.02	1.042

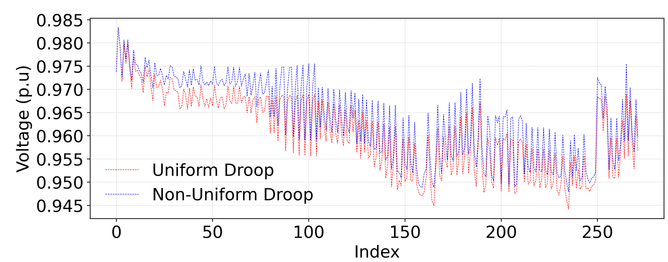

Fig. 7: Voltage of Distributed PV with Droop Configuration 1.

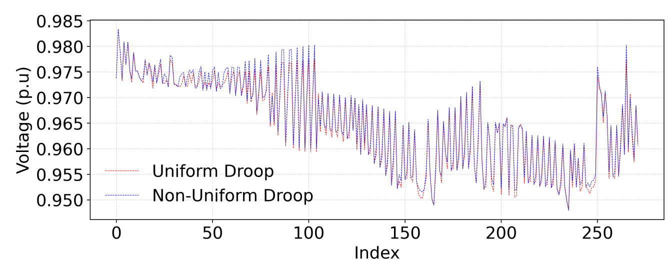

Fig. 8: Voltage of Distributed PV with Droop Configuration 2.

The comparative analysis based on the simulations conducted on the IEEE 123 node feeder reveals that non-uniform droop setting likely achieve faster convergence than uniform droop settings, as shown in Table II. The analysis also indicates that tighter droop coefficients result in improved voltage profile in the distribution feeder.

TABLE II: Convergence of the Algorithm.

Category	Uniform Droop		Non-uniform Droop	
	Config 01	Config 02	Config 01	Config 02
Number of Iterations	64	15	14	7

979-8-3315-8138-1

D. Penetration of Large Scale PVs

The number of PV units is reduced while the individual capacities of the PV are increased, resulting in a total PV capacity of 2.754 MW. Specifically, 500kW PV systems are installed at Bus 7 (phase 'b'), Bus 13 (phase 'b') and Bus 33 (phase 'a'), while 418 kW PV are connected at Bus 63 (phase 'a'), Bus 65 (phase 'c') and Bus 76 (phase 'c') of the IEEE 123 node test feeder (see Fig. 5), resulting in a total of 6 PV installations. This analysis evaluates the voltage profile and power flow convergence for large-scale PV integration. The voltage profiles are evaluated for two distinct configuration setpoints, as specified in Table. I. The voltage profiles for the two configurations are illustrated in Fig. 9 and Fig. 10 for Configuration 01 and Configuration 02, respectively.

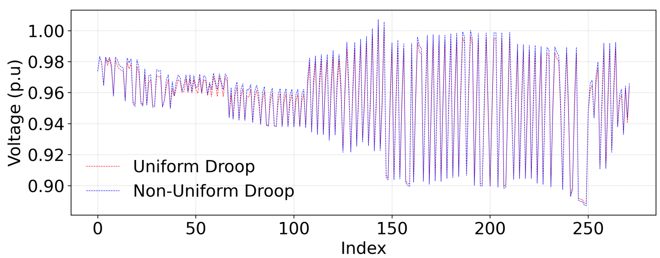

Fig. 9: Voltage of Large-Scale PV with Droop Configuration 1.

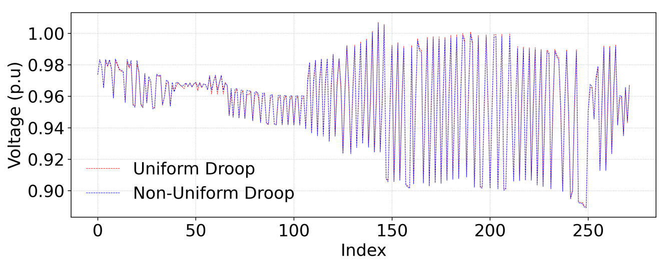

Fig. 10: Voltage of Large-Scale PV with Droop Configuration 2.

For each of the case, the droop settings are implemented either through uniform and non-uniform droop parameters for each SIs. Since, the number of the SI are fewer, the improvement in the voltage is not as great compared to the case of the distributed small Scale PV penetration scenario. A similar observation can be made for the large scale PV case, tighter droop bounds result in better voltage regulation for both of the droop setting configurations (Fig. 10).

TABLE III: Convergence for Droop-enabled Power Flow for Large Scale PV

Category	**Uniform Droop**		**Non-uniform Droop**	
	Config 01	**Config 02**	**Config 01**	**Config 02**
Number of Iterations	36	30	26	5

IV. Conclusion and Future Work

This paper develops a droop-integrated power flow model for unbalanced distribution networks, enabling large-scale DER integration and enabling detailed assessment of voltage impacts under IEEE 1547-compliant droop controls. Two different case studies comparing the uniform and non-uniform droop control settings in the distribution system are analyzed, which shows that well-designed droop settings improve voltage regulation, with non-uniform and varying droop control achieving faster convergence. It provides a practical tool for evaluating voltage support capability, comparing control architectures, and guiding PV deployment under high penetration scenarios. The future research will focus on the scalability and convergence of droop-enabled power flow models in large-scale unbalanced distribution systems. Particular emphasis will be placed on developing well-defined convergence criteria to ensure numerical stability and reliable convergence of the power flow solution algorithm. Droop control functionality will also be extended to Current Injection and Backward-Forward Sweep method of power flow and the models will be also developed for branch- flow based power flow formulations.

References

[1] A. Savasci, A. Inaolaji, and S. Paudyal, "Two-stage volt-var optimization of distribution grids with smart inverters and legacy devices," *IEEE Transactions on Industry Applications*, vol. 58, no. 5, pp. 5711–5723, 2022.

[2] "Renewable capacity statistics 2021," *Tech. Report, International Renewable Energy Agency (IRENA), Abu Dhabi*, 2021.

[3] F. Katiraei and J. R. Agüero, "Solar PV integration challenges," *IEEE Power and Energy Magazine*, vol. 9, no. 3, pp. 62–71, 2011.

[4] "IEEE standard for interconnection and interoperability of distributed energy resources with associated electric power systems interfaces," *IEEE Std 1547-2018 (Revision of IEEE Std 1547-2003)*, pp. 1–138, 2018.

[5] B. Seal and B. Ealy, "Common functions for smart inverters, 4th edition," *Tech. Report, Electric Power Research Institute (EPRI), Palo Alto, CA, 3002008217*, 2016.

[6] B. Seal and B. Ealey, "Common functions for smart inverters, version 3," *Electric Power Research Institute (EPRI)*, 2014.

[7] A. Inaolaji, A. Savasci, and S. Paudyal, "Distribution grid optimal power flow with volt-var and volt-watt settings of smart inverters," in *Proc. IEEE Industry Applications Society Annual Meeting (IAS)*. IEEE, 2021, pp. 1–7.

[8] K. Turitsyn, P. Sulc, S. Backhaus, and M. Chertkov, "Options for control of reactive power by distributed photovoltaic generators," *Proceedings of the IEEE*, vol. 99, no. 6, pp. 1063–1073, 2011.

[9] M. Farivar, R. Neal, C. Clarke, and S. Low, "Optimal inverter var control in distribution systems with high PV penetration," in *Proc. IEEE Power and Energy Society general meeting*, 2012, pp. 1–7.

[10] X. Su, M. A. Masoum, and P. J. Wolfs, "Optimal PV inverter reactive power control and real power curtailment to improve performance of unbalanced four-wire lv distribution networks," *IEEE Transactions on Sustainable Energy*, vol. 5, no. 3, pp. 967–977, 2014.

[11] A. Savasci, A. Inaolaji, and S. Paudyal, "Optimal droop scheduling of smart inverters in unbalanced distribution feeders," in *Proc. IEEE Power Energy Society General Meeting (PESGM)*, 2023, pp. 1–5.

[12] A. Inaolaji, A. Savasci, and S. Paudyal, "Distribution grid optimal power flow in unbalanced multiphase networks with volt-var and volt-watt droop settings of smart inverters," *IEEE Transactions on Industry Applications*, vol. 58, no. 5, pp. 5832–5843, 2022.

[13] A. Neupane and S. Paudyal, "Dynamic droop setting of smart inverters in active distribution grid using neural networks," in *Proc. 56th North American Power Symposium (NAPS)*, 2024, pp. 1–6.

[14] "IEEE Standard for Interconnection and Interoperability of Distributed Energy Resources with Associated Electric Power Systems Interfaces," *IEEE Std 1547-2018 (Revision of IEEE Std 1547-2003)*, pp. 1–138, 2018.

979-8-3315-8138-1